

**ADVANCES IN MODELING COLLISIONS ON ICY BODIES.** S. T. Stewart and L. E. Senft. Dept. of Earth & Planetary Sciences, Harvard University, 20 Oxford St., Cambridge, MA 02138, U.S.A. (sstewart@eps.harvard.edu).

**Introduction:** Impact cratering is one of the major geologic processes on the icy planets and satellites in the solar system. Impact cratering calculations have been used to suggest the presence of transient liquid water [1-4] and to infer the thickness of brittle crusts [5]. These studies rely heavily on the accuracy of (1) the model equation of state of H<sub>2</sub>O to infer the post-impact temperature field and the occurrence of phase changes and (2) the constitutive model to describe the quasi-static and dynamic strength of the material. Here, we present recent advances in the quality of equation of state and constitutive models for H<sub>2</sub>O and implications for collisional processes on icy bodies.

**Equation of State Model:** Because of the complexity of the H<sub>2</sub>O phase diagram, most equation of state (EOS) models used in hydrocode calculations have been tailored to specific phases with little or no ability to extend calculations to broad regions of the phase diagram. In general the phase diagram has been simplified, with one solid phase, liquid, and vapor, such as the ANEOS model described in [5]. Recent development includes an ANEOS-derived tabular multiphase EOS that includes all of the stable solid phases, liquid, and vapor [6].

We have developed a new tabular EOS for H<sub>2</sub>O [7]. The table includes three solid phases (ices Ih, VI, and VII), liquid, and vapor. The EOS of the phases and phase boundaries are experimentally determined. The liquid and vapor are described by the International Association for the Properties of Water and Steam (IAPWS) [8]. The EOS of ice Ih is given by [9]. The EOS of ices VI and VII are taken from [10], and the phase boundaries are given by [8, 11]. The model shock Hugoniots starting as liquid and ice Ih are in excellent agreement with experimental data.

A crucial experimental data set that has been lacking for EOS model validation is shock temperature measurements starting in the ice phase (shock temperatures in liquid water have been measured by [12, 13]). In the Shock Compression Laboratory at Harvard, we have new peak-shock and post-shock temperature measurements in ~150 K polycrystalline ice Ih in the peak shock pressure range of 8.2 to 13.6 GPa [14]. Peak shock temperatures range from 666 to 1044 K and post-shock temperatures are 380 to 495 K. The new tabular EOS is a great improvement over previous EOS models in this pressure range (Fig. 1).

The post-shock temperature provides direct information about the onset and kinetics of shock-induced phase changes. The shock states at these modest pres-

ures are all supercritical (critical point: 647 K, 22 MPa). Under most impact conditions, the isentropic release path intersects the saturation vapor curve. In the  $\mu$ s time scale of the experiments, the observed post-shock temperatures fall on the saturation vapor curve. Further decompression requires the formation of vapor, and the necessary volume expansion is inhibited by the geometry and time scale of the experiment. Transiently hot and pressurized liquid water may lead to interesting dynamic phenomena during crater formation.

The post-shock temperature measurement on the saturation vapor curve defines the entropy in the shock state. Hence, we derive the critical shock pressure required for incipient vaporization to be 8 GPa (3.6 GPa) for release to 1 bar (6 mbar) ambient pressure. The critical shock pressure required for complete vaporization is derived from the new EOS table to be 53 GPa (65 GPa) for release to 1 bar (6 mbar), in excellent agreement with calculations in [10]. Accurate EOS are required to define the initial shock pressure field from the impact and the volumes of shock-induced vapor and melt. Shock-induced vaporization and melting steepen the shock wave decay profile. For ice on ice impacts at 5 km/s and peak pressures around 12 GPa, the power law decay exponent is -1.9 at distances between 2 and 8 projectile diameters. The decay exponent steepens to -3.4 for impacts at 20 km/s and peak pressures of 150 GPa.

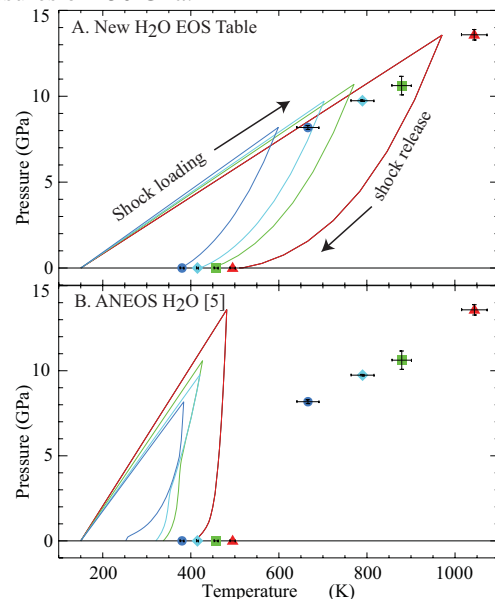


**Fig. 1.** Peak and post-shock temperature data (paired points, [14]) compared with calculated shock loading and release

paths from two different model equations of state (lines).

**Strength Model:** A typical strength model describes the quasi-static response of a material to deviatoric stresses, with weakening due to fracturing (described by a dimensionless damage variable). For crater formation, dynamic weakening processes must also be considered (e.g., acoustic fluidization or frictional melting).

We implemented the quasi-static strength-damage model developed by [15] in the CTH shock physics code [16] and fitted parameters for H<sub>2</sub>O based on laboratory data. In this model, shear strength is linearly degraded from an intact strength value (strength controlled by the creation of new fractures) to a fragmented (strength controlled by friction) value. A dimensionless scalar variable called damage is introduced to track this degradation; completely intact rock has a damage of zero, and completely fragmented rock has a damage of one. Thus, shear strength is a function of damage, temperature, and pressure, and tensile strength is a function of damage.

Strength parameters are chosen by fitting to quasi-static laboratory test data [17-20]. The shear strength data of intact (non-damaged) ice [20] (circles) and the shear strength data of fragmented (damaged) ice [18] (triangles) are compared to the quasi-static strength-damage model in Fig. 2. Note that the strength of ice has a strong temperature dependence. We fit a temperature degradation function to uniaxial compression data from [17] and use this to calculate the strengths at other temperatures. For example, the 210 K intact and damaged shear strength curves are shown in Fig. 2.

Measurements of fresh complex craters on the icy satellites show that these craters are generally much shallower than their lunar counterparts [21, 22], which is expected as a result of the very low coefficient of friction of ice (~0.2 for cold ice, 77 K) as compared to rock (~0.6). Cratering simulations using the quasi-static strength model have shown that craters in pure ice surfaces or rocky surfaces with icy layers have shallow depth to diameter ratios [7, 22].

Furthermore, crater collapse may be aided by frictional melting processes [23, 24]. Frictional melting is observed in laboratory experiments on ice [25] under conditions that should be pervasive during impact events. The dynamic reduction in friction is significant: at a temperature of -10° C, the coefficient of friction of ice approaches 0.001 as the sliding velocity along a fault approaches 1 m/s [25]. Thus, frictional melting effects need to be considered when modeling impacts on icy bodies.

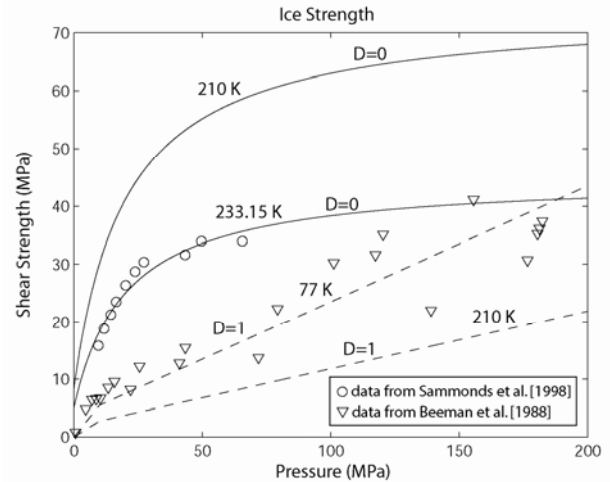


Fig. 2. Shear strength (in terms of the square root of the second invariant of the deviatoric stress tensor,  $\sqrt{J_2}$ ) for fragmented ice (i.e. ice-on-ice friction; dashed lines) and intact ice (solid lines). Also shown are strength curves at 210 K, appropriate for models of cratering on Mars.

**Summary:** We have developed a new multi-phase equation of state for H<sub>2</sub>O and a strength model for ice that are appropriate for the wide range of impact conditions in the solar system. With these advances, we are able to model collisions onto icy bodies with much better accuracy.

**References:** [1] Artemieva, N. and J.I. Lunine (2005) *Icarus* **175**, 522. [2] Artemieva, N. and J. Lunine (2003) *Icarus* **164**, 47. [3] Pierazzo, E., N.A. Artemieva, and B.A. Ivanov (2005) *GSA* **384**, 443. [4] Stewart, S.T., J.D. O'Keefe, and T.J. Ahrens (2004) *Shock Comp. Cond. Mat. - 2003*, 1484. [5] Turtle, E.P. and E. Pierazzo (2001) *Science* **294**, 1326. [6] Ivanov, B.A. (2005) *LPSC* **36**, Abs. 1232. [7] Senft, L.E. and S.T. Stewart (submitted) *MAPS*. [8] Wagner, W. and A. Pruss (2002) *JPCRA* **31**, 387. [9] Feistel, R. and W. Wagner (2006) *JPCRA* **35**, 1021. [10] Stewart, S.T. and T.J. Ahrens (2005) *JGR* **110**, E03005. [11] Frank, M.R., Y.W. Fei, and J.Z. Hu (2004) *Geo. Cos. Acta* **68**, 2781. [12] Kormer, S.B. (1968) *Soviet Physics USPEKHI* **11**, 229. [13] Lyzenga, G.A., et al. (1982) *Jour. Chem. Phys.* **76**, 6282. [14] Stewart, S.T., A. Seifert, and A.W. Obst (2008) *LPSC* **39**, Abs. 2301. [15] Collins, G.S., H.J. Melosh, and B.A. Ivanov (2004) *MAPS* **39**, 217. [16] Senft, L.E. and S.T. Stewart (2007) *JGR* **112**, E11002. [17] Arakawa, M. and N. Maeno (1997) *Cold Reg. Sci. Tech.* **26**, 215. [18] Beeman, M., W.B. Durham, and S.H. Kirby (1988) *JGR* **93**, 7625. [19] Lange, M.A. and T.J. Ahrens (1983) *JGR* **88**, 1197. [20] Sammonds, P.R., S.A.F. Murrell, and M.A. Rist (1998) *JGR* **103**, 21,795. [21] Schenk, P.M. (2002) *Nature* **417**, 419. [22] Bray, V.J., et al. (submitted) *MAPS*. [23] Senft, L.E. and S.T. Stewart (2008) *LPSC* **39**, Abs. 1417. [24] Senft, L.E. and S.T. Stewart (2008) *LMI IV*, Abs. 3077. [25] Maeno, N., et al. (2003) *Can. Journ. Phys.* **81**, 241.